Construction and Building Materials 397 (2023) 132348

Contents lists available at ScienceDirect

Construction and Building Materials

journal homepage: www.elsevier.com/locate/conbuildmat

4D imaging and quantification of the effect of a Phosphate-Based treatment on building materials by means of synchrotron X-ray Microtomography: New insights into the dynamic of the consolidation process

Giulia Massinelli [a,*], Elena Possenti [b], Chiara Colombo [b], G. Diego Gatta [a], Marco Realini [b], Nicoletta Marinoni [a]

[a] Dipartimento di Scienze della Terra, Università degli Studi di Milano, Via Botticelli 23, 20133 Milan, Italy
[b] Istituto di Scienze del Patrimonio Culturale (ISPC), Consiglio Nazionale delle Ricerche (CNR), Via R. Cozzi 53, 20125 Milano, Italy

ARTICLE INFO

Keywords:
Natural stone material
Inorganic consolidants
Consolidation process
Porosity
Diammonium hydrogen phosphate
Synchrotron X-ray Microtomography

ABSTRACT

Diammonium hydrogen phosphate (DAP) solutions are used as consolidants for carbonate stone materials through the crystallization whithin the original matrix of newly formed crystalline phases. However, the formation mechanism of the new phases within the stone microstructure, and their effects on the porous system, strongly depend on the DAP molarity, the treatment method, and the stone microstructure. In this study, we obtained real-time quantitative information on the structural evolutions induced by the treatment process on the Noto limestone, a porous carbonate stone used as a building stone since antiquity, by synchrotron X-ray Microtomography. With the aid of 4D image analysis, microstructural modifications in terms of porosity, interconnection, and pore size distribution have been demonstrated in different stadia of the consolidation process, and the influence of molarity was asserted. This study paves the way for a deeper understanding of consolidation mechanisms and the effects induced overtime on the 3D microstructural features of porous materials by inorganic treatment.

1. Introduction

In the last decades, inorganic-mineral treatments have been considered an effective approch to face the decay of stone materials of Cultural Heritage [1–3]. Treatments based on diammonium hydrogen phosphate ($(NH_4)_2HPO_4$, DAP) have been employed for the conservation of carbonate matrixes [4–8]. DAP solutions dissolve the profile of the original calcite grains of the carbonate substrate leading to the crystallization of new phases (usually calcium phosphates) in a complex mixture [9–11]. As a result, variations are induced in the stone's mineralogical composition and its microstructural features. The newly formed phases, as well as their spatial distribution and the new microstructural features of the DAP-treated stone, strongly depend on the substrate, on the treatment protocol, and on the solution conditions (e.g., pH, molarity) [12–16]. Therefore, the investigation of the formation mechanism of the new phases within the stone structure, and their effects on the porous system, is not at all straightforward [11,17–18].

Although many studies have been performed on DAP treatments, mainly on phase formation and distribution with several analytical techniques, such as Raman spectroscopy, X-ray diffraction, and IR spectroscopy [19–21], the direct effects induced by the solution on the stone microstructure (e.g., pore morphology, connectivity, etc.) are still poorly understood. Moreover, no information is available on the interaction between the calcite crystals and the DAP solution during the reaction process, relevant to understand the timeline of the consolidating mechanism. This study aims to understand the direct effects of DAP solutions on the stone's microstructure through variation of pore morphology, connectivity, and other microstructural features.

In the last years, X-ray Micro-Computed Tomography (μCT) has been applied in the field of material science as it is a spatially resolved technique and offers a 3D overview of the inner part of the samples while also supplying quantitative parameters in a non-invasive way [22–32]. Possenti et al., 2019b [33] has demonstrated the potential of Synchrotron X-ray Micro-Computed Tomography (SR-μCT) in the characterization of the stone microstructure variation due to the treatments by inorganic consolidants, highlighting that phosphates

* Corresponding author.
E-mail addresses: giulia.massinelli@unimi.it (G. Massinelli), elena.possenti@cnr.it (E. Possenti), chiara.colombo@cnr.it (C. Colombo), diego.gatta@unimi.it (G.D. Gatta), nicoletta.marinoni@unimi.it (N. Marinoni).

https://doi.org/10.1016/j.conbuildmat.2023.132348
Received 13 April 2023; Received in revised form 23 June 2023; Accepted 28 June 2023

crystallization modifies the internal microstructure of the lithotype, reducing the total porosity and altering the pore size distribution.

Here, for the first time, real-time SR-μCT has been carried out during the DAP treatment of stone samples with two different molarity (3.0 M and 0.76 M), allowing for a time-lapse of the reaction process. Thanks to a relatively faster acquisition time, it's possible to gain 4D data from the same sample to univocally ascribed the microstructural effects to the crystallization of the new phases within the stone matrix. Unlike traditional porosimetric techniques, the use of synchrotron time-lapse 3D experiments allowed us to work and optimize the near-field free propagation phase contrast, to highlight microstructural features expected in the samples, such as boundary morphology, small porosity, and connectivity. A critical comparison of the 4D evolution of these features within the two DAP solutions' molarity is discussed to gain insight into the dynamic nature of the treatment. This contribution advances the understanding and successful application of inorganic mineral solutions for consolidating treatments in Cultural Heritage preservation.

2. Materials and methods

2.1. Materials

The *Palazzolo Formation limestone*, commonly referred to as "*Noto Limestone*," was selected as a representative lithotype with high porosity within the carbonate rocks [35]. Situated in southeastern Sicily, Italy, it belongs to the Hyblean Plateau, which can be divided into eastern and western sectors. The eastern sector contains Miocene carbonates, limestones, and pyroclastic rocks (Mount Climiti, Palazzolo, and Mount

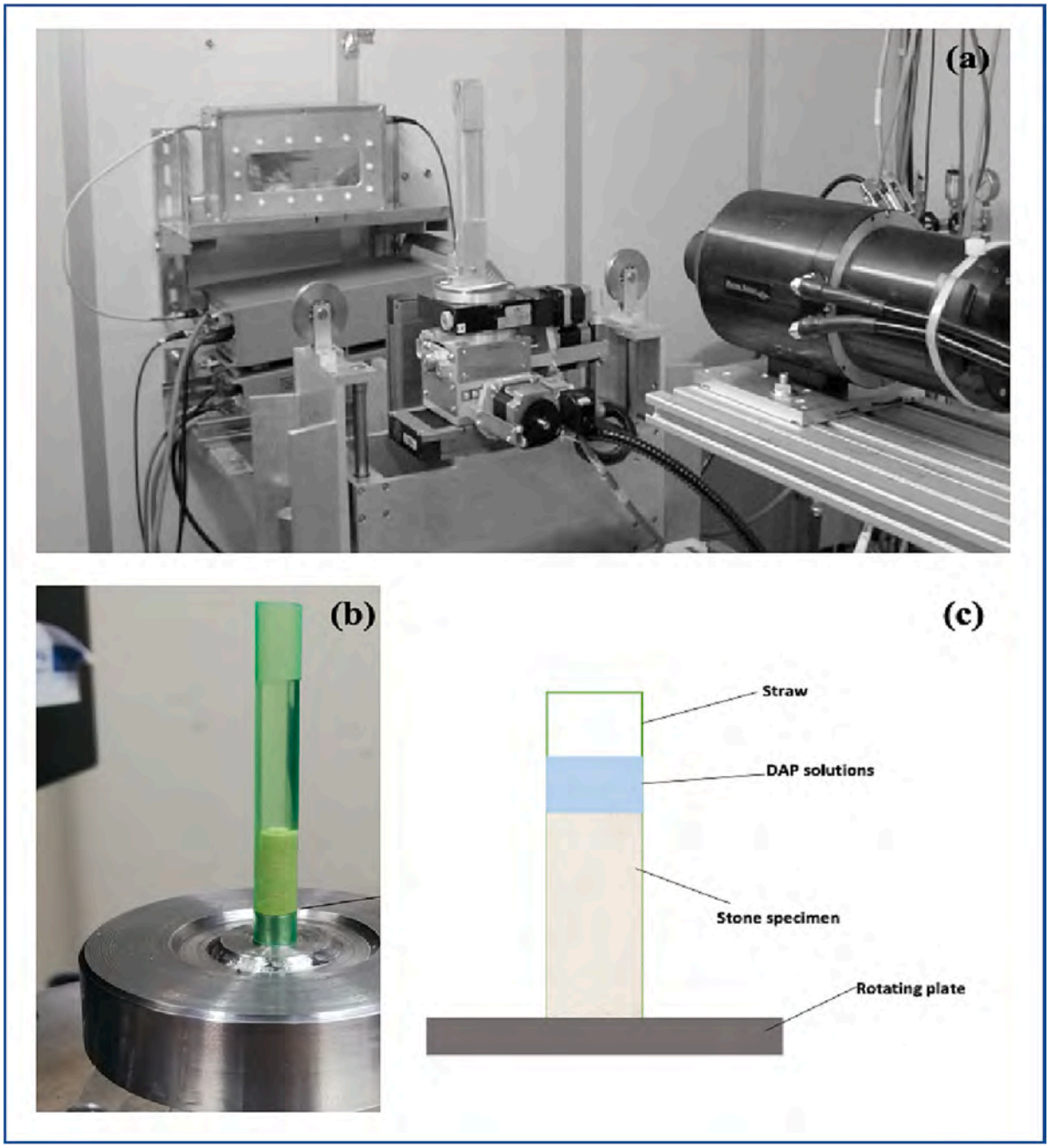

Fig.1. (a) experimental set up @ SYRMEP, ELETTRA synchrotron; (b) zoom of the sample holder containing the straw with the Noto limestone sample and the DAP solution; (c) schematic view of the sample set-up (not in scale).

Carrubba Formations), while the western sector showcases upper Oligocene-Miocene limestone and marl (Ragusa and Tellaro Formations). The Noto Limestone belongs to the former one and corresponds to a marine environment dating back to the Middle to Late Jurassic period [36].

Noto Limestone has been extensively utilized in the construction of historical buildings and monuments in the region, particularly for Baroque structures in the UNESCO World Heritage Site of Noto, Sicily. It is classified as a biomicrite [36], primarily composed of calcite, with subordinate phases including quartz, iron oxides, and clay minerals. The stone's porosity is characterized by micrometric pores, with sizes ranging from 1 to 10 μm and from 1 to 0.1 μm. The porosity of the stone exhibits significant heterogeneity, ranging from 25% to 37% [33,37].

The samples used for the present study were extracted from a freshly quarried block of Noto Limestone and were prepared with a cylindrical shape of 1.5 mm in diameter and 14 mm in height. To minimize the impact of the heterogeneities, we have chosen samples of Noto limestone with the most similar characteristics in terms of microstructure, mineral composition, porosity, water absorption, etc. The selection was carried out using petrographic information and water absorption capillarity tests of the different available samples.

A water-based solution of diammonium hydrogen phosphate (DAP, CAS Number 7783-28-0, assay $\geq$ 99.0%, reagent grade) at two molarities, respectively 0.76 M and 3.0 M, was set according to the previous studies [11,15,20]. An innovative experimental setup was designed *ad hoc* to optimize the interaction between the DAP solutions and the lithotype, allowing the condition of reactivity with ample availability of fluid, as well as enabling high-resolution imaging using synchrotron technology. To achieve this, we utilized a cylindrical sample and placed it onto a straw that was transparent to X-rays. Initially, we conducted a scan of the untreated sample. Then, we introduced DAP solutions by dropping them from the top of the straw using a syringe until the sample was completely submerged (see Fig. 1b and c). We monitored the treatments for a duration of 24 h, following the methodology used in previous studies [38,39].

The samples were labeled 0.76M and 3M; in this paper, a second part is added to the label (0 h, 1 h … and so on) meaning the time (hours) from the beginning of the treatment in which the images have been acquired.

2.2. Methods

2.2.1. Synchrotron radiation X-ray Micro-Computed Tomography (SR-μCT)

Synchrotron radiation X-ray Micro-Computed Tomography (SR-μCT) was used to investigate *in* real-time the influence of DAP treatments on the 3D pore network [40] to gain 4D imaging of the samples. SR-μCT experiments were carried out at the SYRMEP (Synchrotron Radiation for Medical Physics) beamline at the Elettra Synchrotron facility in Basovizza (Trieste), Italy.

The X-ray SR-μCT experiments were performed by 'pink' beam mode at a median energy of 27 keV, with a Si filter of 1.5 mm and an Al filter of 1.0 mm to optimize the X-ray spectrum for the experiment; the sample-to-detector distance was set at 150 mm. The detector used was an air-cooled, 16-bit, sCMOS camera. Measurements were carried out with an effective pixel size of the detector set at 0.9 × 0.9 μm^2, yielding a maximum field of view of about 1.8 × 1.8 mm^2. The exposure time/projection was 2.5 s. Since the lateral size of the samples was larger than the detector field of view, the scans were acquired in local or region-of-interest mode. The Noto limestone samples were placed onto a high-resolution rotation stage with a constant angular step.

Initially, the SR-μCT scans were performed on the dry samples to investigate the porous microstructure of the untreated lithotype. Then the DAP treatments were applied and several SR-μCT datasets were taken at different times during the consolidation process. For the dry samples, 1800 X-ray projections were acquired, whereas for the treated samples only 900 projections were collected. In this latter case, the acquisition of 900 high-quality images within a reasonable time (~50 min) allowed us to monitor any potential change in the sample.

2.2.2. Data processing

The tomographic projections were processed with the SYRMEP Tomo Project (STP) software suite, developed in-house at Elettra, to perform the CT reconstruction employing the Filtered Back-Propagation algorithm. A single-distance phase retrieval algorithm was applied to projection images before CT reconstruction [41]. A filter for ring removal was used to reduce the artifacts in the reconstructed slices. A brightness and contrast correction filter was also applied to homogenize the images resulting in a widely distributed signal intensity of the images.

The software *ImageJ* was used to visualize the slices and select three representative Volumes of Interest, VOI, per sample [42,43] (Fig. 2a). To provide representative VOI dimension, REV (Representative Elementary Volume, REV) sizes were determined by using the box-counting method, consisting of the study of the variation of pore volume fraction for increasing sub-volumes [44,45]. For our data, a cubic increase of 4 voxels in lateral size was considered until a reasonable plateau. In this study, a satisfactory representative volume was defined of 600 × 600 × 600 voxels (corresponding to a cube of ~ 540 μm side length). The VOIs were selected at different depths of the samples to consider the occurrence of microstructural differences. The reported values used in the study were derived from the mean of the data obtained from the analysis of three subvolumes extracted from the same sample, ensuring a more robust and representative characterization of the sample's properties.

Variations in gray values observed among different regions indicate the presence of distinct chemical compositions, densities, or both. To effectively analyze the imaging data, ranges of gray values were established for different phases, enabling the segmentation of the data into microporous regions filled with solution and the stone/new products system. This segmentation process, known as image segmentation, was performed using thresholding based on Otsu's selection method. This method was chosen because it fulfilled two criteria: 1) it included over 98% of the voids within the desired range, and 2) the segmented images closely matched the raw images.

The outcome of the segmentation process was the generation of binary images, where similar elements were represented as sets of contiguous voxels. Since the porous stones exhibited isolated pores, the connected porosity was extracted from the resulting binarized volumes using the "Find connected regions" tool provided by the software.

The *Pore3D software library*, developed by the SYRMEP research group of Elettra for analysis of porous media, was used to obtain quantitative information for a better understanding of the microstructure and establish interrelationships between properties [43]. From the segmented volume, the Minkowski functionals (or basic parameters) were computed. In this study, our focus was two Minkowski functionals: *(i)* Volume density (V_V), which here represents the porosity, and *(ii)* Euler characteristic (C_V or X_V), which is an index of connectivity of the pores network which provides us with a value of the connectedness of the 3D pores network [46]. To capture the morphological variations, a blob analysis was implemented, which calculates direct 3D statistics on connected regions in a binary image. Among the obtainable data, we focused on the volume values (the volume of each identified blob computed as the number of voxels rescaled according to the specified voxel size [mm^3]). The measured pore volumes were divided into classes according to the IUPAC pore size classification (approximated to a system of sphere-shaped volumes). The obtained counts were fitted as a normal distribution; hence, pore size distribution variations were estimated.

Lastly, a skeleton (or medial axis) of the microstructure was generated following the LKC method contained within the Pore3D software library, thus allowing a topological characterization of the interconnected voids. The LKC Skeletonization computes the skeleton of a 3D binary image using the Lee, Kashyap, and Chu algorithm [46] reducing

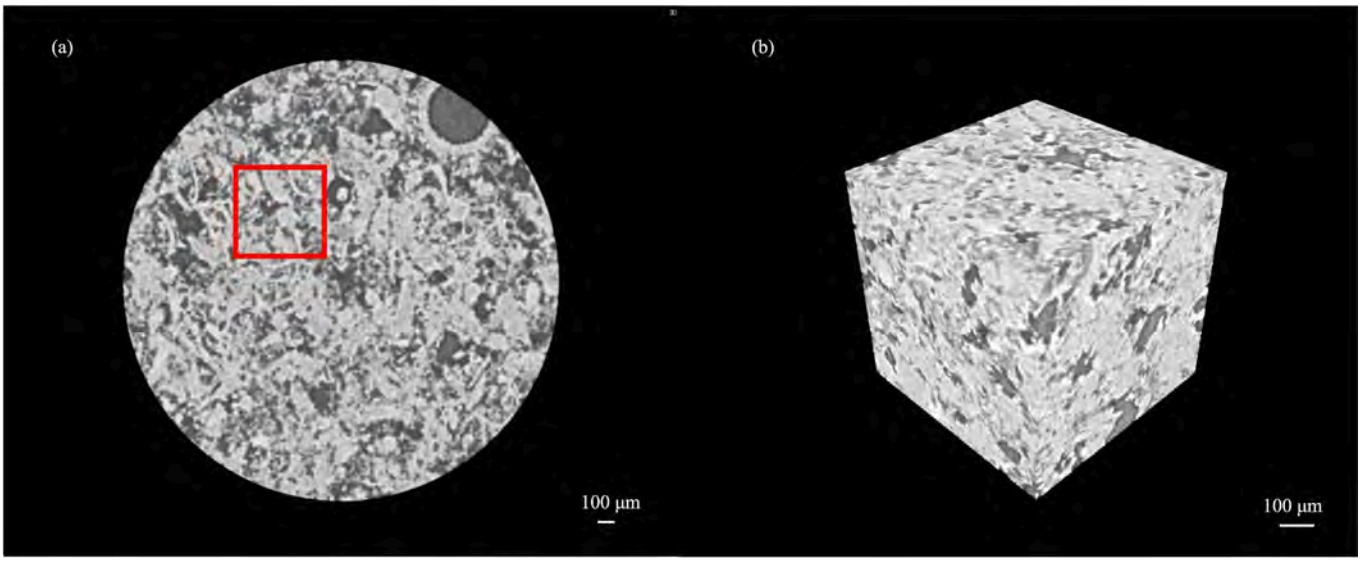

Fig. 2. Reconstructed images: (a) a two-dimensional (2D) frontal slice of the 3M_0h Noto Limestone sample obtained from synchrotron X-ray microtomography at the SYRMEP beamline of Elettra and the selected region of interest (red box). (b) Volume rendering of the VOI, 600 × 600 × 600 voxel with a voxel size of 0.9 × 0.9 × 0.9 μm^3. (For interpretation of the references to colour in this figure legend, the reader is referred to the web version of this article.)

them to a network of nodes and branches that preserves the features of the original object. The algorithm has been applied to a binary smoothed version of the segmented image to reduce the complexity of branches.

The visualization of the reconstructed pores network was performed by 3D rendering procedures using the commercial software *VGStudio 3.1.2* (Fig. 2b). The original binary images of the total porosity were pre-processed with a higher median filter (i.e., 10) to reduce the contribution of isolated voxels and simplify the information. Renderings of the skeletons were also obtained using the commercial software.

3. Results

In Fig. 3, the SR-μCT slices of a VOI of the 3.0 M DAP-treated Noto limestone are shown during each step of the reaction process (i.e., from untreated up to 24 h of treatment). The untreated lithotype (Fig. 3. a) is characterized by pores of variable size and angular morphologies. In the slices of the DAP-treated sample, the pores' morphology is regular and smoother, already after 1 h of treatment (Fig. 3. b).

In addition to the pore's morphological variations, the SR-μCT images allow us to recognize another trend: the closure of the throats. In Fig. 4, a deeper insight into the voids in 3M_0h and 3M_1h are compared. It is worth noting that the grayscale values along the voids are different, as clearly illustrated by the line profile of the greyscale corresponding to a red and black line marked in Fig. 4a and b, respectively. After 1 h of treatment inside the pores, the lighter part corresponds to the newly formed crystal phases, whereas the darker one corresponds to the remaining voids, with the presence of newly formed phases inside the voids. So, these variations are ascribable to the formation of CaPs at the interface between the grain boundary and the solution due to the reaction of calcite.

Focusing on the following stages of the treatment process, we notice that the modification trend of the pore's edges and their morphology continues over 24 h. The smoothing of the pore results in the creation of pores smaller in size in the treated sample compared to the untreated lithotype. This transition towards a microporosity reduced in dimensions is further supported through a local thickness 2D distance map. These maps provide valuable preliminary insights into the spatial size distribution of the porosity as it is generated from the diameter of the largest sphere that fits inside the voids. By modeling the local thickness, in the 3M_1h sample, a higher number is registered of spheres

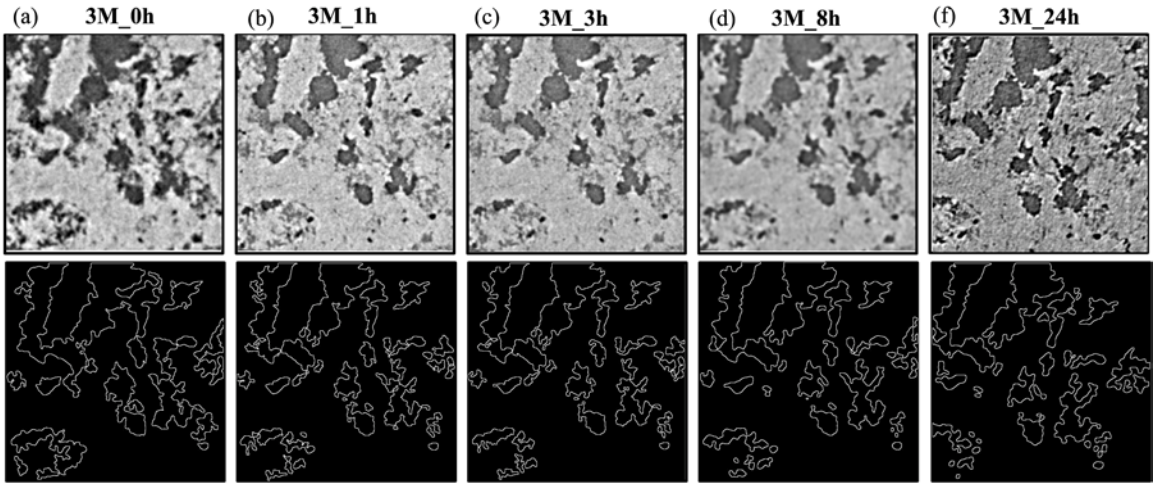

Fig. 3. Outline (in white) of the main pores in a 600 × 600 voxel^2 area through time on the 3.0 M DAP solutions treated limestone surface: 3M_0h (before treatment) (a), 3M_1h (b), 3M_3h (c), 3M_8h (d) and 3M_24h (e) (end of treatment).

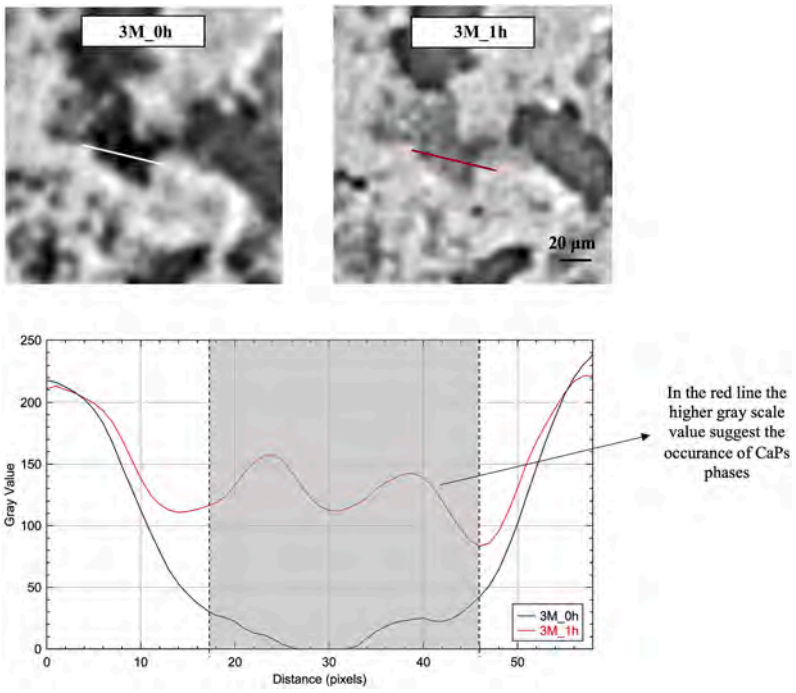

Fig. 4. Grayscale values profile of a pore showing the lithotype before the treatment (3M_0h) and the CaPs crystallization at the grain boundary after 1 h of treatment (3M_1h) only.

with smaller dimensions meaning a decrease in the size of the pores (Fig. 5).

In Fig. 6, the slices of 0.76 M treated substrate, from the untreated stage up to 7 h of treatment, are shown. Like the other molarity, the pores on the 1 h - treated matrix are smothered and have less branching (i.e., the connection between pores).

In this SR-µCT study, the total porosity of the untreated sample has been asserted at ~ 34 % (Table 1). The data has shown that, in the untreated lithotype, approximately 97% of the total porosity is composed of a system of open and interconnected cells (Table 1, Connected porosity). The 3.0 M−treated sample after 1 h shows a total porosity reduction of ~ 33 %. Hence, the 3.0 M solution results in a material with a lower porosity than the untreated one. The 3-hour volume, on the other hand, underwent a slight increase in total porosity, being now ~ 30% less than the untreated sample. After about 8 h, the data underline again a reduction in the total porosity. This descendent trend is maintained till the end of the treatment (24 h), resulting in an overall reduction of the microporosity of around 40%.

Focusing on the connected components ("open porosity") of the stone microstructure, the porous network in the VOIs is asserted by the morphometric analysis and explored by the 3D renderings and skeleton analysis (Fig. 7). The treated porous microstructure in all VOIs remains

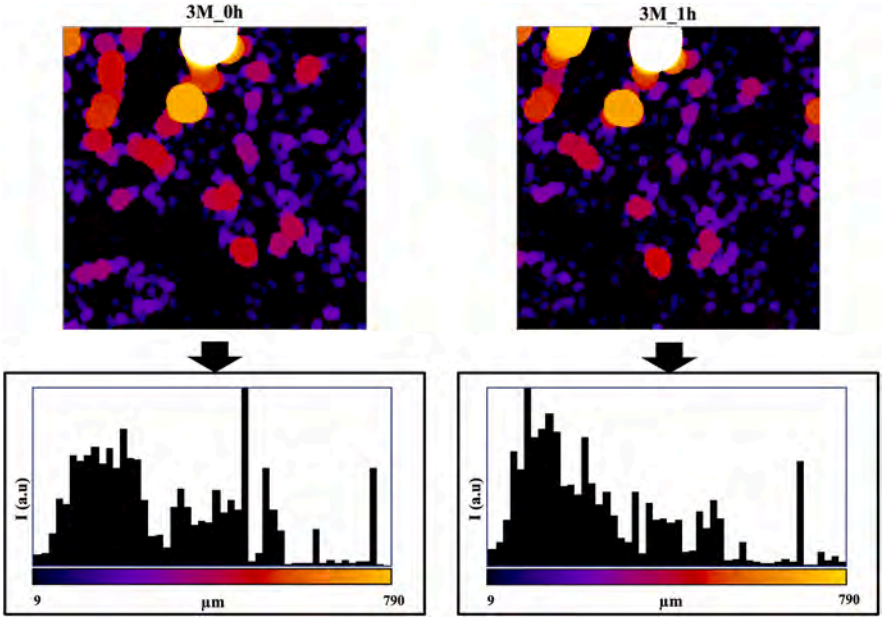

Fig. 5. Local Thickness 2D distance maps and respective histograms showing the distribution of the pore size in the sample untreated (3M_0h) and after 1 h of treatment (3M_1h).

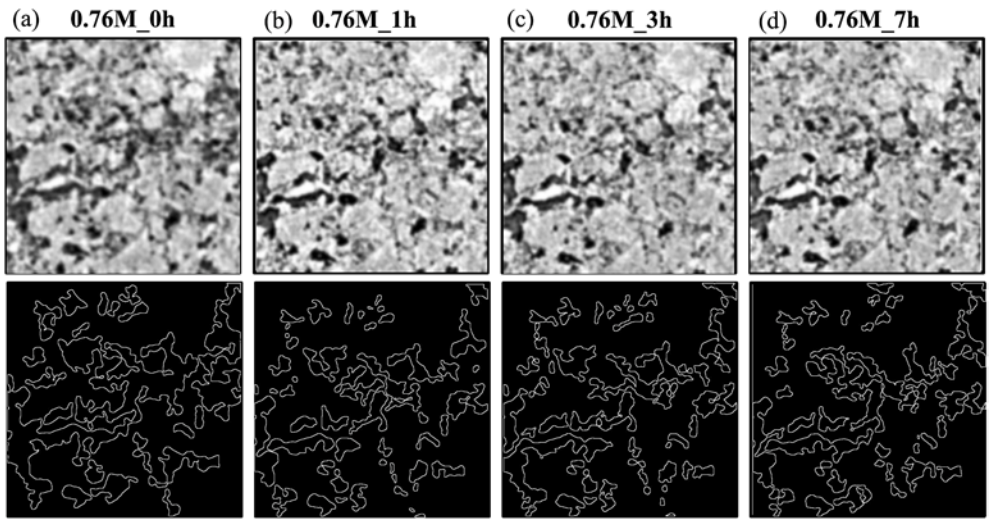

Fig. 6. Outline (in white) of the main pores in a 600 × 600 voxel^2 area through time on the 0.76 M DAP solutions treated limestone surface: 0.76M_0h (before treatments) (a), 0.76M_1h (b), 0.76M_3h (c), 0.76M_7h (d).

Table 1
Morphometric analysis. The arithmetic mean (AM) is indicated for values obtained with the morphometric analysis on the 3.0 M and 0.76 M DAP-treated samples. The standard deviation is ± 3% of the mentioned value.

Time Stamp (hours)	Total porosity (vol. %)		Connected porosity (vol. %)	
	3.0 M	*0.76* M	*3.0* M	*0.76* M
0	34	34	33	33
1	21	23	18	22
3	23	24	22	23
7–8	22	24	20	23
24	21	–	19	–

characterized by an open complex system of branching throughout the 3.0 M treatment process.

In the 0.76 M−treated sample, a decrease in total porosity to the untreated one is maintained as well during the overall process. After 1 h the porosity reduction is of a similar magnitude (~33 % less) if compared to the one resulting from the 3.0 M solution and a slight increase is registered at the 3rd hour. Contrary to the higher molarity, however, this molarity does not restrain a descendent trend throughout the full path of the process, i.e., total porosity still undergoes a slight increase starting from the third hour. Nonetheless, at the end of the treatment, the resulting 0.76 M−lithotype presents a lower porosity than the untreated one around 30%. Like the other molarity, the crystallization of the phases does not seem to occlude the porous network but maintains an open and interconnected system (Fig. 8).

To study the pore distribution, the pore volume size was extracted by blob analysis. The extrapolated data generated two cumulative curves showing the evolution of the pore in the VOIs, in terms of pores numbers and occupied volume (Figs. 9 and 10). The untreated volumes appear as a highly interconnected network of pores composed of a main "large volume" and some smaller pores, of variable number and size. In the 3.0 M−treated sample, after 1 h, the "large volume" decreases by half, which can be related to the increase in the number of small and medium pores (volume between 1.00 E^{01} μm^3 and 1.00 E^{05} μm3). The 'set back' (i.e., the third-hour increase) found in the morphometric analysis is also found in the porosimetric analysis, as there is a reduction in the number of medium and small pores in the third-hour data followed by an increase in the 8-hour volume, which is maintained till the end of the treatment. Similarly, the sample treated with 0.76 M exhibits a reduction of the large volume, and subsequently increase of pores, with volumes between 1.00 E^{01} μm^3 and 1.00 E^{05} μm^3 during the first hour of treatment. The trend is not maintained for the rest of the treatment time. However, with both molarities, a variation in the pore volume occurs, which results in a final lithotype with a higher number of small and medium pores, if compared to the parental material.

4. Discussion

The morphometric measurements obtained provide compelling evidence that DAP solutions have a significant impact on the microstructure of the stone material. Additionally, the microstructural modifications induced by the DAP treatments highlight a strong time-dependent nature, regardless of the solution molality. This revealed that the process is highly dynamic with the most significant changes occurring within the first hour of treatment. This means that most of the carbonate matrix dissolution and subsequent crystallization of newly formed phases on pore walls occur within the first hour. The reaction dynamics are, therefore, faster than the expected ones, and further investigations are surely needed to explore the reactions occurring during the first hour with a faster acquisition.

The analysis indicates that the crystallization process occurs preferentially within the microporosity, specifically on the pore boundaries and throats, influencing the overall porous network. However, the stone matrix during the treatment is still characterized by a system of highly interconnected communicating channels, which govern the interaction with fluids.

The results of the blob analysis further confirm that the treatment process induces variations in pore size distribution compared to the untreated matrix. Specifically, the treated Noto limestone specimens exhibit a higher number of small and medium-sized pores. The difference between the rate of increasing small porosity may lie in the reduction of the initial "large pores". The high-resolution volume renderings reveal that the actual micropore system is characterized by strong connectivity through thin channels, pore-to-end branches, and irregular borders. It is important to note that although this analysis was crucial for exploring micropore variations, the resolution limitations of the imaging technique made it challenging to detect sub-micrometric pores and channels, resulting in a portion of the microporosity falling below the detection limit (e.g., Noto Limestone pores with a diameter < 1 μm account for approximately 7% [32]). Furthermore, the connection of regions by a few pixels, owing to the 0.9 μm pixel size of the scan, and the use of image filters may cause highly interconnected pores to be incorrectly identified as part of a single "large volume". Nevertheless, a lower total open porosity and a different pore size distribution to the

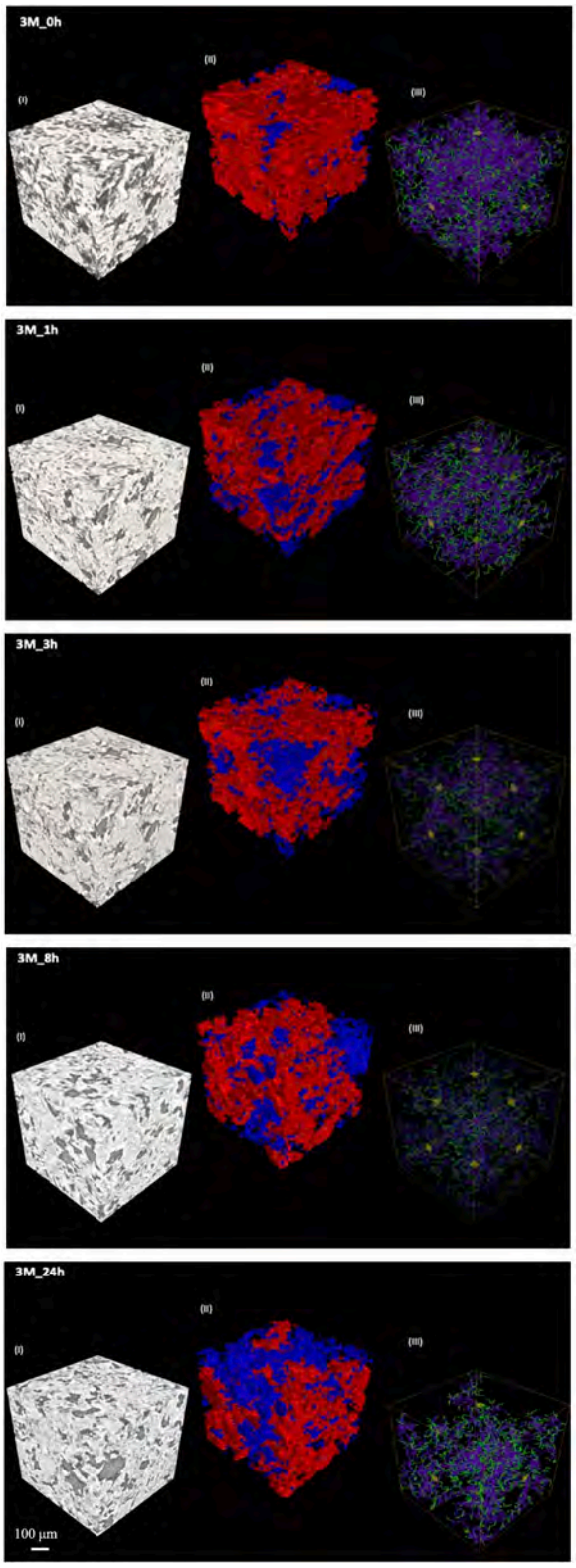

Fig. 7. Volume renderings of 3 M DAP-treated Noto limestone VOI: parallelepiped cropped close to the surface (600 × 600 × 600 voxels). The renderings include (I) X-ray tomographic images, (II) a combination of connected (red) and isolated (blue) pores, and (III) the connected pores skeleton (node-to-node component in violet and node-to-end component in green) of treated Noto limestone. The orange cube represents the VOI. (For interpretation of the references to colour in this figure legend, the reader is referred to the web version of this article.)

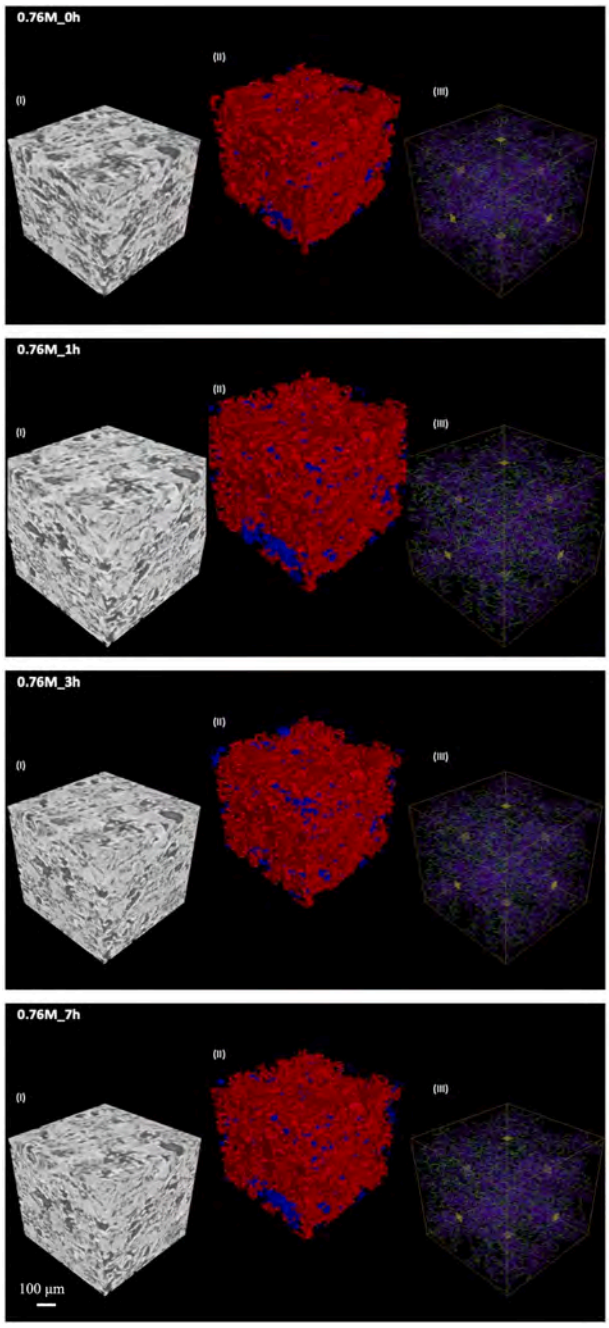

Fig. 8. Volume renderings of 0.76 M DAP-treated Noto limestone VOI: parallelepiped cropped close to the surface (600 × 600 × 600 voxels). The renderings include (I) X-ray tomographic images, (II) a combination of connected (red) and isolated (blue) pores, and (III) the connected pores skeleton (node-to-node component in violet and node-to-end component in green) of treated Noto limestone. The orange cube represents the VOI. (For interpretation of the references to colour in this figure legend, the reader is referred to the web version of this article.)

untreated matrix are coherent with previous studies [33–34] and confirm that the differences depend on the DAP consolidating treatment.

Examining the treatment dynamics, it is evident that the morphological and porosity variations are not uniform throughout the treatment duration for both molarities. In the case of the 3.0 M DAP solution, we observed a "first reaction" step, characterized by significant modifications occurring within a short timeframe. This step is followed by a period without notable effects, as evidenced by the standstill recorded in the morphometric and porosimetric data at the third hour of treatment.

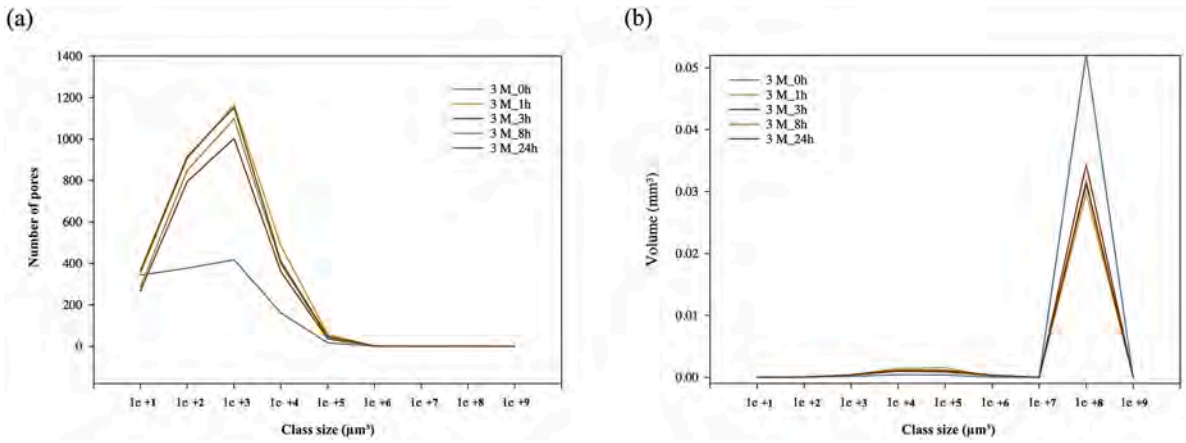

Fig. 9. Comparison of the cumulative distribution functions of the number of pores (a) and of volumes (b) on the 3.0 M DAP-treated samples.

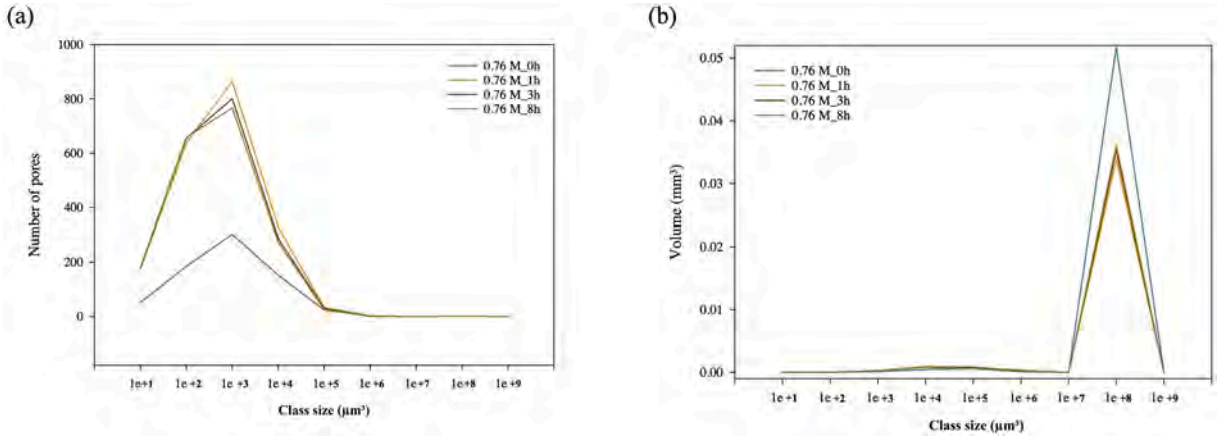

Fig. 10. Comparison of the cumulative distribution functions of the number of pores (a) and of volumes (b) on the 0.76 M DAP-treated samples.

Subsequently, a "second reaction" phase commences around the eighth hour of treatment, marked by additional dissolution and the generation of new voids. The "second reaction" culminates in the crystallization within these "new voids," which modifies the stone microstructure, yielding effects like those observed during the initial reaction, albeit with less pronounced magnitude (Fig. 11).

On the other hand, according to the interpretations made in the Results, the 0.76 M DAP solution exhibited a different reaction mechanism. Although it had lower molarity and can dissolve the calcite substrate, it still triggered a fast dissolution and crystallization process at the beginning of the treatment, with a milder impact on microstructure morphology and porosity. After the third hour of treatment, a plateau is reached, indicating a lack of further changes. The consumption of the reagent and the formation of more stable phases could both be possible to consider as possibilities for this different behavior. Also, a neutralization in the solution pH happens inside the pores during the reaction process, a shift towards acidity can inhibit the reaction with limestone. However, the real role of the pH during the reaction is difficult to assert due to the instrumental impossibility of measuring its value inside the micropores. In addition, many of the consolidating phases (mainly hydroxyapatite [15,33]) are characterized by low solubility in water, which could prevent a second action on the treated system with the inhibition of corrosion phenomena in lower molarity. These data, although they acknowledge the influence of solution molarity on the modifications to the microstructure, they also highlight that molarity does not necessarily correlate with the reaction and crystallization process rate. Further investigation is needed to explore reaction kinetics and the resulting microstructural changes, especially in the time frame where most changes occur.

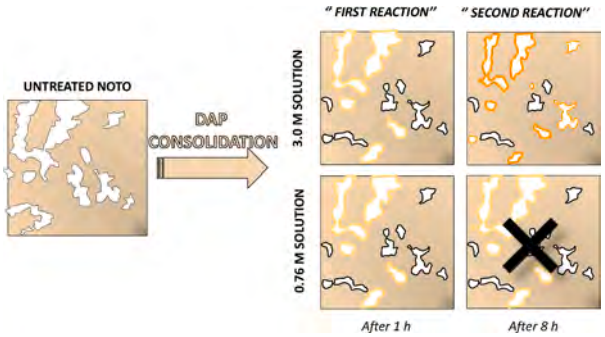

Fig. 11. Schematic diagram of reaction processes that the lithotype experiences when treated with different molarity of DAP solution. In yellow are the changes given by the "first reaction" and in orange are the ones caused by the "second reaction" in the 3.0 M DAP treated sample (absent for the 0.76 M treated sample). (For interpretation of the references to colour in this figure legend, the reader is referred to the web version of this article.)

5. Conclusions

In conclusion, the present research highlights the significance of SR-µCT as a powerful tool for investigating both qualitative (visualization of consolidating processes, pore smoothing, etc.) and quantitative (calculation of porosity, estimation of dimensional changes, computation of interconnectivity, etc.) inorganic mineral treatments on carbonate

rocks. The study revealed also significant findings regarding the dynamics of DAP consolidating treatments. The distribution of CaPs phases formed during the treatments results in a transformation of the internal microstructure, particularly within the first hour of treatment, leading to a less porous lithotype while maintaining a high degree of interconnectivity, characterized by an increased number of small voids. The qualitative and quantitative analysis of the 4D data of the reconstructed volume renderings provides comprehensive insights into the evolution of a treated porous network: factors such as boundary morphology, total porosity, distribution, and connectivity, which play a crucial role in assessing the effectiveness of DAP consolidating treatments, particularly in outdoor conditions. The dynamic nature of the treatment reveals distinct reaction phases dependent on the DAP molarity, underscoring the importance of solution properties in the observed microstructural changes.

This research opens many questions, especially on the relationship between solution molarity, reaction kinetics, and the dynamic evolution of pore edges within a tighter time frame. Ongoing reasearchs aim for a more comprehensive understanding of the microstructural dynamics, phase transformations, and chemical composition during the DAP treatment. Also, by integrating with diffraction techniques, we aim at obtaining mineralogical and crystallographic information of the newly formed CaPs formed phases and their spatial distribution; which would enhance our understanding of how microstructural changes affect the new crystallin products and vice versa.

In summary, the findings of this study contribute significantly to our understanding of how inorganictreatments influence the porous network and provide crucial insights for optimizing their performance in stone conservation.

CRediT authorship contribution statement

Giulia Massinelli: Formal analysis, Writing – original draft, Writing – review & editing, Data curation. **Elena Possenti:** Conceptualization, Investigation, Methodology, Writing – original draft, Writing – review & editing. **Chiara Colombo:** Formal analysis, Writing – original draft, Writing – review & editing. **G. Diego Gatta:** Writing – original draft, Writing – review & editing. **Marco Realini:** Investigation, Resources, Writing – original draft, Writing – review & editing. **Nicoletta Marinoni:** Funding acquisition, Supervision, Writing – original draft, Writing – review & editing.

Declaration of Competing Interest

The authors declare that they have no known competing financial interests or personal relationships that could have appeared to influence the work reported in this paper.

Data availability

No data was used for the research described in the article.

Acknowledgements

The authors acknowledge the Elettra Synchrotron, Trieste (Italy) for allocation of experimental beamtime at SYRMEP (SYnchrotron Radiation for MEdical Physics) (proposal n. 20190090) and Dr. Lucia Mancini who assist us during the experiments and Giovanni Possenti for his support in the design and realization of the *ad hoc* sample holder.

Author Contributions

G.M., E.P., C.C. and N.M. wrote the main manuscript text. E.P. and M.R. performed the CT analysis and G.M., E.P., N.M and C.C. interpreted the results. All authors (G.M. E.P., C.C., D.G. M.R.) assisted in the revision of the initial draft of the manuscript.

Funding sources

This research did not receive any specific grant from funding agencies.

References

[1] M. Matteini, Inorganic treatments for the consolidation and protection of stone artifacts, Conserv. Sci. Cult. Heritage 8 (2008) 13–27, https://doi.org/10.6092/issn.1973-9494/1393.
[2] M. Matteini, S. Rescic, F. Fratini, G. Botticelli, Ammonium phosphates as consolidating agents for carbonate stone materials used in architecture and cultural heritage: preliminary research, Int. J. Archit. Heritage 5 (6) (2011) 717–736, https://doi.org/10.1080/15583058.2010.495445.
[3] E. Sassoni, S. Naidu, G.W. Scherer, The use of hydroxyapatite as a new inorganic consolidant for damaged carbonate stones, J. Cult. Herit. 12 (4) (2011) 346–355, https://doi.org/10.1016/j.culher.2011.02.005.
[4] B.S. da Fonseca, A.F. Pinto, S. Piçarra, B. Caldeira, M.F. Montemor, Consolidating efficacy of diammonium hydrogen phosphate on artificially aged and naturally weathered coarse-grained marble, J. Cult. Herit. 51 (2021) 145–156, https://doi.org/10.1016/j.culher.2021.08.003.
[5] J. Menningen, E. Sassoni, R. Sobott, S. Siegesmund, Constraints of the durability of inorganic and organic consolidants for marble, Environ. Earth Sci. 80 (2021) 1–18, https://doi.org/10.1007/s12665-021-09664-w.
[6] E. Sassoni, E. Franzoni, Lime and cement mortar consolidation by ammonium phosphate, Constr. Build. Mater. 245 (2020), 118409, https://doi.org/10.1016/j.conbuildmat.2020.118409.
[7] A. Murru, R. Fort, Diammonium hydrogen phosphate (DAP) as a consolidant in carbonate stones: impact of application methods on effectiveness, J. Cult. Herit. 42 (2020) 45–55, https://doi.org/10.1016/j.culher.2019.09.003.
[8] S.E. Celik, J. Gulen, H.A. Viles, Evaluating the effectiveness of DAP as a consolidant on Turkish building stones, Constr. Build. Mater. 262 (2020), 120765, https://doi.org/10.1016/j.conbuildmat.2020.120765.
[9] E. Sassoni, G. Graziani, E. Franzoni, An innovative phosphate-based consolidant for limestone. Part 1: effectiveness and compatibility in comparison with ethyl silicate, Constr. Build. Mater. 102 (2016) 918–930, https://doi.org/10.1016/j.conbuildmat.2015.04.026.
[10] G. Graziani, E. Sassoni, G.W. Scherer, E. Franzoni, Penetration depth and redistribution of an aqueous ammonium phosphate solution used for porous limestone consolidation by brushing and immersion, Constr. Build. Mater. 148 (2017) 571–578, https://doi.org/10.1016/j.conbuildmat.2017.05.097.
[11] E. Possenti, C. Colombo, D. Bersani, M. Bertasa, A. Botteon, C. Conti, P.P. Lottici, M. Realini, New insight on the interaction of diammonium hydrogen phosphate conservation treatment with carbonate substrates: a multi-analytical approach, Microchem. J. 127 (2016) 79–86, https://doi.org/10.1016/j.microc.2016.02.008.
[12] L. Wang, G.H. Nancollas, Calcium orthophosphates: crystallization and dissolution, Chem. Rev. 108 (11) (2008) 4628–4669, https://doi.org/10.1021/cr0782574.
[13] A.P.F. Pinto, J.D. Rodrigues, Consolidation of carbonate stones: influence of treatment procedures on the strengthening action of consolidants, J. Cult. Herit. 13 (2) (2012) 154–166, https://doi.org/10.1016/j.culher.2011.07.003.
[14] E. Franzoni, E. Sassoni, G. Graziani, Brushing, poultice, or immersion? The role of the application technique on the performance of a novel hydroxyapatite-based consolidating treatment for limestone, J. Cult. Herit. 16 (2) (2015) 173–184, https://doi.org/10.1016/j.culher.2014.05.009.
[15] E. Possenti, C. Colombo, C. Conti, L. Gigli, M. Merlini, J.R. Plaisier, M. Realini, D. Sali, G.D. Gatta, Diammonium hydrogen phosphate for the consolidation of building materials. Investigation of newly formed calcium phosphates, Constr. Build. Mater. 195 (2019) 557–563, https://doi.org/10.1016/j.conbuildmat.2018.11.077.
[16] E. Possenti, C. Conti, G.D. Gatta, M. Merlini, M. Realini, C. Colombo, Synchrotron radiation μ X-ray diffraction in transmission geometry for investigating the penetration depth of conservation treatments on cultural heritage stone materials, Anal. Methods 12 (12) (2020) 1587–1594, https://doi.org/10.1039/D0AY00010H.
[17] E. Sassoni, G. Graziani, E. Franzoni, Repair of sugaring marble by ammonium phosphate: comparison with ethyl silicate and ammonium oxalate and pilot application to the historic artifact, Mater. Des. 88 (2015) 1145–1157, https://doi.org/10.1016/j.matdes.2015.09.101.
[18] G. Masi, E. Sassoni, Air lime mortar consolidation by nano limes and ammonium phosphate: compatibility, effectiveness, and durability, Constr. Build. Mater. 299 (2021), 123999, https://doi.org/10.1016/j.conbuildmat.2021.123999.
[19] Graziani, G., Sassoni, E., Scherer, G. W., & Franzoni, E. (2018, June). Phosphate-based treatments for consolidation of salt-bearing Globigerina limestone. In IOP Conference Series: Materials Science and Engineering (Vol. 364, No. 1, p. 012082). IOP Publishing. 10.1088/1757-899X/364/1/012082.
[20] E. Sassoni, Hydroxyapatite and other calcium phosphates for the conservation of cultural heritage: a review, Materials 11 (4) (2018) 557, https://doi.org/10.3390/ma11040557.
[21] A. Defus, E. Possenti, A. Sansonetti, C. Tedeschi, C. Colombo, D. Biondelli, S. Vettori, M. Realini, Di-ammonium hydrogen phosphate for the consolidation of lime-based historic mortars–Preliminary research, J. Cult. Herit. 48 (2021) 45–53, https://doi.org/10.1016/j.culher.2021.01.005.
[22] J. Dewanckele, T. De Kock, M.A. Boone, V. Cnudde, L. Brabant, M.N. Boone, G. Fronteau, L. Van Hoorebeke, P. Jacobs, 4D imaging and quantification of pore

structure modifications inside natural building stones by means of high-resolution X-ray CT, Sci. Total Environ. 416 (2012) 436–448.
[23] V. Cnudde, A. Cwirzen, B. Masschaele, P.J.S. Jacobs, Porosity and microstructure characterization of building stones and concretes, Eng. Geol. 103 (3–4) (2009) 76–83, https://doi.org/10.1016/j.enggeo.2008.06.014.
[24] V. Cnudde, M.N. Boone, High-resolution X-ray computed tomography in geosciences: a review of the current technology and applications, Earth Sci. Rev. 123 (2013) 1–17, https://doi.org/10.1016/j.earscirev.2013.04.003.
[25] V. Cnudde, T. De Kock, M. Boone, W. De Boever, T. Bultreys, J. Van Stappen, D. Vandevoorde, J. Dewanckele, H. Derluyn, V. Cárdenes, L. Van Hoorebeke, Conservation studies of cultural heritage: x-ray imaging of dynamic processes in building materials, Eur. J. Mineral. 27 (3) (2015) 269–278.
[26] V. Brunello, C. Canevali, C. Corti, T. De Kock, L. Rampazzi, S. Recchia, A. Sansonetti, C. Tedeschi, V. Cnudde, Understanding the microstructure of mortars for cultural heritage using X-ray CT and MIP, Materials 14 (20) (2021) 5939.
[27] R. Ševčík, A. Viani, L. Mancini, M.S. Appavou, D. Machová, Investigation of nano-microstructural changes in Maastricht limestone after treatment with nano lime suspension, Appl. Phys. A 126 (5) (2020) 367, https://doi.org/10.1007/s00339-020-03567-6.
[28] M. Slavíková, F. Krejčí, J. Žemlička, M. Pech, P. Kotlík, J. Jakůbek, X-ray radiography and tomography for monitoring the penetration depth of consolidants in Opuka–the building stone of Prague monuments, J. Cult. Herit. 13 (4) (2012) 357–364, https://doi.org/10.1016/j.culher.2012.01.010.
[29] T. Bultreys, L. Van Hoorebeke, V. Cnudde, Multi-scale, micro-computed tomography-based pore network models to simulate drainage in heterogeneous rocks, Adv. Water Resour. 78 (2015) 36–49, https://doi.org/10.1016/j.advwatres.2015.02.003.
[30] N. Marinoni, M. Voltolini, M.A.T.M. Broekmans, P.J.M. Monteiro, L. Mancini, N. Rotiroti, E. Ferrari, A. Bernasconi, Combined synchrotron radiation micro-computed tomography and micro-X-ray diffraction study on deleterious alkali-silica reaction, J. Mater. Sci. 50 (2015) 7985–7997, https://doi.org/10.1007/s10853-015-9364-7.
[31] V. Caruso, N. Marinoni, V. Diella, F. Berna, M. Cantaluppi, L. Mancini, L. Trombino, C. Cattaneo, L. Pastero, A. Pavese, Bone diagenesis in archaeological and contemporary human remains an investigation of bone 3D microstructure and mineral-chemical assessment, Archeological and Anthropological Sciences 12 (2020) 162, https://doi.org/10.1007/s12520-020-01090-6.
[32] N. Marinoni, M. Voltolini, L. Mancini, F. Cella, Influence of aggregate mineralogy on alkali–silica reaction studied by X-ray powder diffraction and imaging techniques, J. Mater. Sci. 47 (2012) 2845–2855, https://doi.org/10.1007/s10853-011-6114-3.
[33] E. Possenti, C. Colombo, C. Conti, N. Marinoni, M. Merlini, R. Negrotti, M. Realini, G.D. Gatta, Consolidation of building materials with a phosphate-based treatment: t Effects on the microstructure and the 3D pore network, Mater Charact 154 (2019) 315–324, https://doi.org/10.1016/j.matchar.2019.05.037.
[34] E. Possenti, C. Conti, G.D. Gatta, N. Marinoni, M. Merlini, M. Realini, G.B. M. Vaughan, C. Colombo, Synchrotron X-ray diffraction computed tomography to non-destructively study inorganic treatments, Science 25 (2022), 105112, https://doi.org/10.1016/j.isci.2022.105112.
[35] R. Punturo, L.G. Russo, A.L. Giudice, P. Mazzoleni, A. Pezzino, Building stone employed in the historical monuments of Eastern Sicily (Italy). An example: the ancient city center of Catania, Environ. Geol. 50 (2006) 156–169, https://doi.org/10.1007/s00254-006-0195-3.
[36] G. Barbera, B. Germana, V. Crupi, F. Longo, G. Maisano, D. Majolino, P. Mazzoleni, S. Raneri, J. Teixeira, V. Venuti, A multi-technique approach for the determination of the porous structure of building stone, Eur. J. Mineral. 26 (1) (2014) 189–198, https://doi.org/10.1127/0935-1221/2014/0026-2355.
[37] G. Barone, V. Crupi, F. Longo, D. Majolino, P. Mazzoleni, S. Raneri, J. Teixeira, V. Venuti, Neutron radiography for the characterization of porous structure in degraded building stones, J. Instrum. 9 (05) (2014) C05024–C.
[38] E. Possenti, C. Conti, G.D. Gatta, M. Merlini, M. Realini, C. Colombo, Synchrotron radiation m X-ray diffraction in transmission geometry for investigating the penetration depth of conservation treatments on cultural heritage stone materials, Anal. Methods 12 (12) (2020) 1587–1594, https://doi.org/10.1039/D0AY00010H.
[39] E. Possenti, C. Colombo, M. Realini, C.L. Song, S.G. Kazarian, Time-resolved ATR–FTIR spectroscopy and macro-ATR–FTIR spectroscopic imaging of inorganic treatments for stone conservation, Anal. Chem. 93 (44) (2021) 14635–14642, https://doi.org/10.1021/acs.analchem.1c02392.
[40] A. Abrami, F. Arfelli, R.C. Barroso, A. Bergamaschi, F. Billè, P. Bregant, F. Brizzi, K. Casarin, E. Castelli, V. Chenda, L. Dalla Palma, D. Dreossi, C. Fava, R. Longo, L. Mancini, R.-H. Menk, F. Montanari, A. Olivo, S. Pani, A. Pillon, E. Quai, S. Ren Kaiser, L. Rigon, T. Rokvic, M. Tonutti, G. Tromba, A. Vascotto, C. Venanzi, F. Zanconati, A. Zanetti, F. Zanini, Medical applications of synchrotron radiation at the SYRMEP beamline of ELETTRA, Nucl. Instrum. Methods Phys. Res., Sect. A 548 (1-2) (2005) 221–227.
[41] F. Brun, L. Massimi, F. Fratini, D. Dreossi, F. Billé, A. Accardo, R. Pugliese, A. Cedola, SYRMEP Tomo project: a graphic user interface for customizing CT reconstruction workflows, Ad. Struct. Chem. Imaging 4 (2017), https://doi.org/10.1186/s40679-016-0036-8.
[42] I.M. Gitman, H. Askes, L.J. Sluys, Representative volume: existence and size determination, Eng. Fract. Mech. 74 (2007) 2518–2534, https://doi.org/10.1016/j.engfracmech.2006.12.021.
[43] F. Brun, L. Mancini, P. Kasae, S. Favretto, D. Dreossi, G. Tromba, Pore3D: a software library for quantitative analysis of porous media, Nucl. Instruments Methods Phys. Res. Sect. An Accel. Spectrometers, Detect. Assoc. Equip. 615 (2010) 326–332, https://doi.org/10.1016/j.nima.2010.02.063.
[44] M.S. Costanza-Robinson, B.D. Estabrook, D.F. Fouhey, Representative elementary volume estimation for porosity, moisture saturation, and air-water interfacial areas in unsaturated porous media: data quality implications, Water Resour. Res. 47 (7) (2011), https://doi.org/10.1029/2010WR009655.
[45] R. Al-Raoush, A. Papadopoulos, Representative elementary volume analysis of porous media using X-ray computed tomography, Powder Technol. 200 (1–2) (2010) 69–77, https://doi.org/10.1016/j.powtec.2010.02.011.
[46] Brun, F. (2012). Development of algorithms and methods for three-dimensional image analysis and biomedical applications. http://hdl.handle.net/10077/7736.